Proceedings of 10th IOE Graduate Conference
Peer Reviewed
ISSN: 2350-8914 (Online), 2350-8906 (Print)
Year: 2021 Month: October Volume: 10

Urban Heat Island: A case study of Kathmandu Valley

Bishnu Chaudhary [a], Inu Pradhan Salike [b], Khem Naryan Poudyal [c]

[a, c] *Department of Applied Science and Chemical Engineering, Pulchowk Campus, IOE, Tribhuvan University, Nepal*
[b] *Department of Architecture, Pulchowk campus, IOE, Tribhuvan University, Nepal*
Corresponding Email: [a] cybishnu216@gmail.com, [b] inupradhan@gmail.com, [c] khem@ioe.edu.np

Abstract

Rapid urbanization influences the local climate, making cities warmer than it's countryside and woodland areas, increase in frequency and magnitude extreme climatic events, that exploits the healthy living environment.Land Use Land Cover (LULC) change influences physical properties of soil and hydrological cycle, eventually alter the temperature. This study focus on the study of surface temperature and Urban Heat Island (UHI) of Kathmandu valley distinctly in Kathmandu, Bhaktapur, and Lalitpur district, as a result of the use of remote sensing and ArcGIS in respect of cities, and countryside and woodland areas. The Landsat 8 satellite's Operational Land Imager (OLI) and Thermal Infrared (TIR) bands were applied to evaluate urban heat islands. Mono window Algorithm (MWA) is used to estimation of land surface temperature. 6 weather station temperature data were used to validate analyzed land surface temperature from satellite remote sensing and GIS. Result shows urban sprawl influence on spatial distribution of land surface temperature and existence of hot spot in the central areas of the Kathmandu valley. Central zone of the valley experiences high surface temperature in respect of the neighbouring rural areas. Dense built up areas has significantly higher temperature than the vegetative and water bodies ares.

Keywords

Urban Heat Island (UHI), Land Surface Temperature (LST), Land Use Land Chnage (LULC), Remote sensing, Mono Window Algorithm (MWA)

1. Introduction

Kathmandu Valley is a highly populated city center comprising of the town of Kathmandu, Bhaktapur, and Lalitpur district. Anthropogenic activities highly influence Land Use and Land Cover [1]. Modification and alternation of land cover areas leads to natural environment degradation, changes is urban hydrology, increment of warmness, climate change from local to regional [2]. Urban regions encounters higher surface and air temperature than neighbouring rural and suburban regions, leads to creation of Urban Heat Island (UHI) [3]. UHi is generally affected by substitution of land surfaces by imprevious [4]. Very first time urban heat island was reported by Howard in 1818 [5].

Utilization of energy and consumption of water has been increased due to effect of UHI. Mainly there is reduction in air quality levels and high energy demands during summer seasons. For the temperature above 15-20°C, energy demand escalate by 2 to 4% for every 1°C rise in the diurnal maximum temperature [6]. This generally happens due to increased energy demand for cooling UHI leads to high pollutant concentration in city areas and it impacts the micro climate by altering pattern of the wind, increasing humidity, formation of fog and clouds and alternation rainfall pattern [7, 8]. Smog formations are highly accelerated due to hot airs in urban areas [9].

High surface, and air temperature in the urban areas are due to high built up density in respect to the surrounding sub urban and rural areas, this difference in temperature is termed as UHI. Different satellite sensors are used for remote sensing to analyze the UHI effect. Likewise ground based measurements has been used for various studies. In 1972, for the first time pointed out UHI observation using satellite based sensor, afterward numbers of satellites have been used for remote observation [10]. Different satellites are used for thermal remote sensing to study surface urban heat island [11]. Advanced Very High Resolution Radiometer (AVHRR), Moderate

Resolution Image Specroradiometer (MODIS), Huan Jing (HJ-1B), Landsat, and Advanced Spaceborne Thermal Emission and Reflection Radiometer (ASTER) are used for spatial and temporal analysis as they have beneficial spatial coverage, temporal repetition and low cost [12]. Landsat data produces much more convincing result with higher accuracy than AVHRR and MODIS [13]. Earth's surface skin temperature is termed as Land Surface Temperature (LST). Increase in LST is mainly due to interlinking of both earth's surface and atmosphere energy [14]. Substantial increase in temperature and about 0.74 Kelvin rise in mean global land surface temperature has been reported by Intergovernmental Panel on Climate Change [15]. Formation of hot spot (HS) and higher LST are mainly due to build up areas. Urban areas development intensity can be analyzed through measurement of impervious surface area and increase of this leads to growth of urban areas [16]. Likewise cold spot has low temperature due to open and vegetative areas and thus forms cool island [17]. Evapotranspiration and shades from trees and vegetation also reduces the temperature in urban areas and leads to reduction in surface heat island [18]. Higher portion of impervious surfaces such as built up areas with low albedo and lower vegetative areas leads to high intensity UHI [19]. There is reduction of 1.3°C in LST as per 10% increase of vegetative areas [20].

As urban areas increases, there is reduction in vegetative areas and this leads to increase in surface temperature [21]. Huge urbanization, population increment and economic growth as main factors behind growth of UHI. United Nations [22] has projected 9.1 billion population by 2050, and about 70% of the population will be residing in urban areas. Thus rise of population and urbanization growth will continuing in future along with magnitude of UHI effects [23]. Study of UHI provides understanding about UHI occurrence, and it's geographical growth and spatial distribution, which can be used in UHI mitigating strategies on both local and global climate. Therefore, maintaining healthy living environment it becomes necessary to analyze surface urban heat island and identify it's spatial distribution.

Number of LST estimation algorithm has been created for LANDSAT 8 data using thermal band data [24]. Mono-window calculation is one of the widely utilized method for surface temperature assessment [25]. To analyze LST from the band 10 information of Landsat 8 satellite images, ArcGis is used. Parameters like atmospheric transmittance, ground emissivity and average effective atmospheric temperatures are also necessary for LST analysis. TIR sensor of Landsat 8 is used to quantify skin temperature of earth's surface. Likewise NOAA (National Oceanic and Atmospheric Administration)-AVHRR (Advanced Very High Resolution Radiometer) sensor, Terra and Aqua satellite-MODIS (Moderate Resolution Imaging Spectroradiometer), ASTER (Advanced Space borne Thermal Emission and Reflection Radiometer, and Landsat are used for LST quantification.

Visible Red band i.e. band 4, and Near Infrared band i.e. band 5 data of Landsat 8 satellite OLI sensor are used for quantification of Normalized Difference Vegetation Index (NDVI), which characterizes number of vegetation properties of land. NDVI index ranges from -1 to +1 and uses for classification of land cover [26]. Study areas land cover is classified in to built up areas, vegetation, water bodies, and barren land. Present study focus on feasibility of finding LULC using band 1-7, data from OLI sensor and LST by using band10 data from TIR sensor of LANDSAT 8. Mono Window Algorithm is used for quantification of land surface temperature, and urban heat island of Kathmandu valley. After finding LST using band10 then it is compared with the weather station data. Finally statistical tool method used was used to determine correlation coefficient [27]. Emissivity of land surface is also very much requisite to quantify the temperature of land surface. For determining emissivity, proportion of vegetation must be determined and at first NDVI must be estimated to estimate proportion of vegetation. For this analysis ArcGIS 10.5 software is used to process Landsat 8 Satellite data.

2. Research Objective

The focus of this studies is to examine at land surface temperature and urban heat island with in Kathmandu valley via analyzing at Kathmandu, Bhaktapur, and Lalitpur districts separately.

3. Study Area

This study is conducted in Kathmandu valley with area of 695 km2 [28]. Total area with Kathmandu, Bhaktapur, and Lalitpur district is 933.73 km2, Kathmandu valley is in shape of bowl basin [29], surrounded by Shivapuri hills, Pulchowki, Nagarjun and Chandragiri. The North latitude of Kathmandu valley ranges in between 27°31´55″to 27°48´56″and East longitude ranges in between 85°11´11″to 85°31´52″[30]. It has been most rapidly growing urban agglomeration in south-Asia [31]. As per census of 2011, 2,517,023 was the total population of Kathmandu valley was among which 1,465,254 were residing in urban areas with annual population growth of 4.78 percentage in 2011. Kathmandu valley shares 24 percentages of total urban population of the country and Kathmandu Metropolitan City (KMC) alone accounts 9.7 percentage of total urban population [32]. Although urbanization and population growth in Kathmandu valley has been increasing abruptly, but lack of proper planning and haphazard infrastructure development is adding constraints and setbacks for sustainable development in Kathmandu valley.

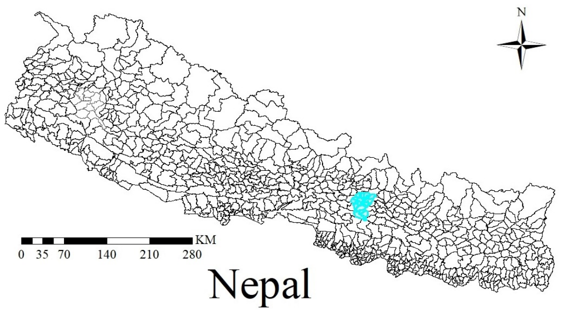

Figure 1: Map of Nepal

Topography of Kathmandu valley is complicated as inside a small geographical area, it is elevated from 1,100-2,700 meters [33]. "This tectonic valley is a Tertiary structural basin protected through fluvial and lacustrine sediments, and encircled by using mountains on all aspects" [33]. The local weather of Kathmandu valley is sub-tropical cool temperate. Average winter temperature 10ºC and Average summer temperature 30ºC [33]. Study on temperature trend from five weather station of Kathmandu valley from 1971-2011 found increase rate of 0.33°C in mean temperature, 0.043°C in maximum and 0.02°C in minimum temperature [34]. Most of the rainfall takes place between June and August as an end result of southeast monsoon winds. Some rainfall takes place all through the winter, added by way of alternate winds from the northwest [35]. Annual humidity in the valley is about 75%. The valley is drained by means of the Bagmati river system. The river gadget is the main source of water for ingesting and irrigation in the valley [30].

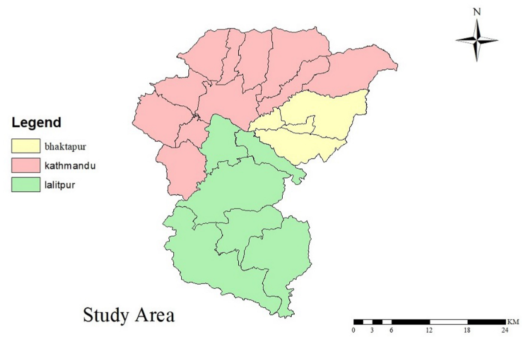

Figure 2: Study Area of Kathmandu Valley

4. Methodology

4.1 Image Classification

Measurement of meteorological parameters requires TIRS and OLI bands of Landsat 8 OLI/TIRS. Multispectral and multiple band images of LANDSAT 8 satellites were downloaded from website of USGS earth explorer [36]. Earths every point are crossed and captured by Landsat 8 satellite in every 16 days. OLI and TIRS sensor provide information in 11 spectral bands. Image is selected based on path and row information. Hence, here 143/51 chosen which is the path/row of the study area is selected for the LST estimation purpose and this swath covers area of Kathmandu, Bhaktapur, and Lalitpur district. Image for the date 10th March, 2020 (LANDSAT 8 Collection -1 and Level -1 of OLI/TIR) were chosen for Land Surface Temperature estimation. The images were selected with minimum cloud cover so that most of the image area is suitable for study purpose. The framework of this study is shown in figure 3.

4.2 Land Use Land Cover Classification

Band 1-7, of Landsat 8 OLI sensor are used to for the classification of land use land cover. ArcGIS 10.5 combines all these seven OLI bands of Landsat 8 to form composite bands for land cover classification. Raster clipping of the Kathmandu, Bhaktapur, and Lalitpur districts are done to mask out the thesis study area. Training samples were taken for vegetation, built up areas, barren lands, and water bodies to classify land use land cover. After then supervision classification is done and land use land cover of Kathmandu valley is classified.

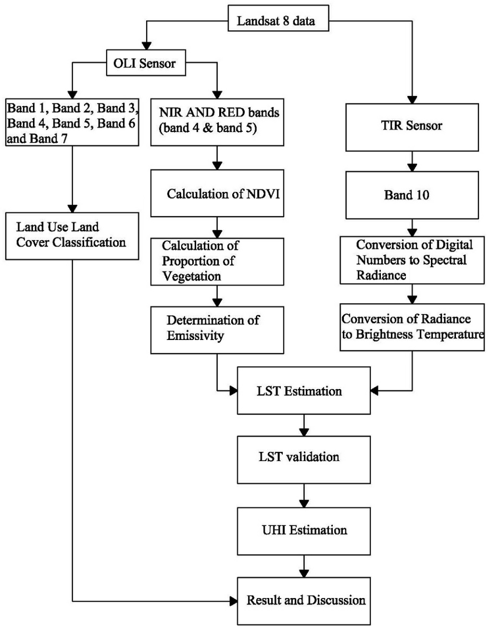

Figure 3: Research Framework

4.3 Land Surface Temperature Calculation

Estimation of LST in Kathmandu valley is the propose work of this study,i.e. in Kathmandu, Bhaktapur, and Lalitpur district by using Landsat 8 satellite band 10 independently through usage Mono Window Algorithm. Mono Window algorithm has 6 steps for quantification LST. These steps are only for Landsat 8 and Landsat 8 satellite data are processed using this steps. Before LST quantification, brightness temperature value must be determined which is then followed by determination of land surface emissivity and then NDVI value. Mono window algorithm step uses Thermal Infra-Red sensor band 10 of LANDSAT 8 satellite [37, 38] independently. After calculation of land surface temperature via band 4, band 5, and band 10, it is needed to validate from in-suite temperature data collected from weather stations. The LST estimation through remote sensing and ArcGIS is compared with in-suite weather stations temperature data. Eventually, correlation coefficient for LST and Weather data is computed and analyzed.

The steps of the Mono Window Algorithm for LST estimation using ArcGIS 10.5 are as follows:

Step 1

Translation of satellite image Digital Number (DN) into spectral radiance called Top of Atmosphere (TOA) is done by applying the equation number (1) and the band specific parameters are presented in the Table 1. These parameters obtained from metadata file.

$$L\lambda = ML * Qcal + AL \tag{1}$$

Where;

$L\lambda$: Spectral radiance of TOA (mW /sr mm2)

ML: Multiplicative rescaling value

AL: Additive rescaling factor of specific band

Qcal: Digital Number (i.e. Quantized and calibrated pixel values)

Table 1: Band 10 Specific Parameters

Parameters	Band 10
ML	0.0003342
AL	0.1

Step 2

Conversion of Top of Atmosphere (TOA) radiance into brightness temperature (BT) by using $L\lambda$ and band specific thermal conversion constants K1 and K2 specified in metadata file of satellite image. The resultant temperature is obtained in Kelvin. It is converted into Celsius by adding -273.15°C i.e. absolute zero. Brightness temperature in Celsius is estimated by the equation (2). The thermal conversion constants are shown in table 2.

$$BT = \frac{K2}{ln(k1/L\lambda + 1)} - 273.15 \tag{2}$$

Where;

BT: Brightness Temperature in degree Celsius

$L\lambda$: Top of Atmospheric spectral radiance (Band 10)

K1 and K2: Thermal Sensor constants used for conversion (Source: metadata file)

Table 2: Thermal conversion constants

Parameters	Band 10
K1	774.8853
K2	1321.0789

Step 3

The OLI (Operational Land Imager) sensor spectral images of bands 4 and 5 used for calculating NDVI

(Normalized Difference Vegetation Index). The NDVI values vary between -1.0 to +1.0. That depends on the various objects on the land surface which is going to be captured by the sensor. NDVI of each pixel is estimated by using Red band i.e. band 4 and Near Infrared band i.e. band 5 of LANDSAT 8 by using the equation no. (3)

$$NDVI = \frac{NIR - RED}{NIR + RED} \tag{3}$$

Where;

RED: DN values of RED band

NIR: DN values of Near-Infrared band

Calculation of NDVI is necessary for estimation of vegetation proportion (PV) and land surface emissivity (LSE i.e. E) parameter which are needed for estimating the Land Surface Temperature.

Step 4

Vegetation proportion (PV) is calculated by using equation number 4, where NDVI is obtained from step 3.

$$PV = \frac{(NDVI - NDVImin)^2}{(NDVImax - NDVImin)^2} \tag{4}$$

Where;

PV: Proportion of Vegetation

NDVI: DN values from NDVI Image

NDVImin: Minimum DN values of NDVI Image

NDVImax: Maximum DN values of NDVI Image

After the estimation of NDVI values of study area, then consider from that NDVI image lowest and highest values of the NDVI image.

Step 5

Land Surface Emissivity (E) anticipated through the use of the NDVI threshold method. LSE is essential parameter for calculating the LST, because it is a proportionality thing that is used to scale blackbody radiance, so that emitted radiance can be predicted. Moreover, it's capability of passing on thermal energy throughout the surface and in to the atmosphere [27]. Therefore the land surface emissivity (E) is computed by using the equation no (5).

$$E = 0.004 * PV + 0.986 \tag{5}$$

Where;

E = Land Surface Emissivity

PV = Proportion of Vegetation

Where;

0.004 - Standard deviation of soil bands,

0.989 - Average Emissivity (i.e average of soil and vegetation emissivity factors)

Step 6

The ultimate step of estimating the LST is by using the equation (6)

$$LST = \frac{BT}{1 + (\frac{W * BT * ln(E)}{14380}} \tag{6}$$

Where;

BT = Top of atmosphere brightness temperature (°C)

W = Wavelength of emitted radiance

E = Land Surface Emissivity

4.4 Urban Heat Island Calculation

Urban heat island is the case in which temperature of city area is higher than the it's countryside and woodland areas. UHI can be calculated using equation 7 in the raster calculator.

$$UHI = \frac{Ts - Tm}{S.D.} \tag{7}$$

Where;

Ts: Land Surface Temperature of study area (°C)

Tm: Mean of Land Surface Temperature (°C)

S.D.: Standard deviation of LST

5. Results and Discussion

5.1 Land Use Land Cover

Land use land cover maps were derived from composite band i.e combination of band 1-7 of OLI sensor of Landsat 8 OLI/TIRS. Maximum likelihood classifier (MLC) is used to assign pixels based on. Image classification is done in to four categorr i.e. Built up areas, Vegetation, Water bodies, and Barren land. For assessment of accuracy confusion matrix and signature file is used [39]. Overall accuracy in Kathmandu, Bhaktapur, and Lalitpur district was 88.48%, 85.63%, and 86.25% respectively, and Kappa coefficient was 0.846, 0.808, and 0.817 for Kathmandu, Bhaktapur, and Lalitpur respectively. Figure 4, figure 5, and figure 6 illustrates LULC of Kathmandu, Bhaktapur, and Lalitpur district respectively. Table 3, table 4, and table 5 shows the area and percentage coverage of built up areas, water bodies, barren lands, and vegetation cover areas of Kathmandu, Bhaktapur and Lalitpur districts respectively.

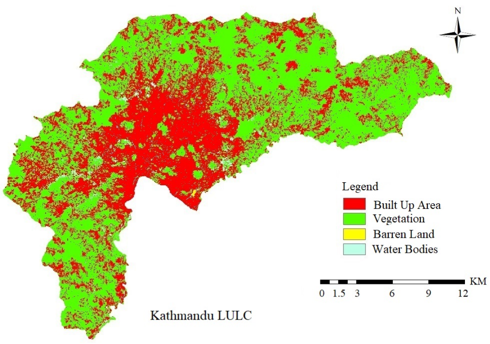

Figure 4: Land Use Land Cover map of Kathmandu district

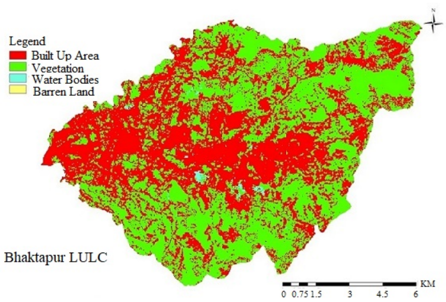

Figure 5: Land Use Land Cover map of Bhaktapur district

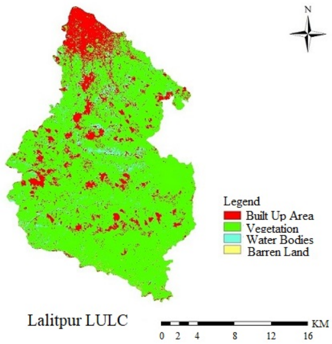

Figure 6: Land Use Land Cover map of Lalitpur district

Table 3: Land Use Land Cover Classification of Kathmandu district: 10th March, 2020

Class Name	Area (sq. km.)	Percentage
Barren Land	17.71	0.04
Built Up Area	152.46	0.37
Vegetation	238.27	0.58
Water Bodies	5.00	0.01
Total	413.44	1.00

Table 4: Land Use Land Cover Classification of Bhaktapur district: 10th March, 2020

Class Name	Area (sq. km.)	Percentage
Barren Land	15.20	0.12
Built Up Area	51.91	0.42
Vegetation	54.12	0.44
Water Bodies	1.81	0.02
Total	123.04	1.00

Table 5: Land Use Land Cover Classification of Lalitpur district: 10th March, 2020

Class Name	Area (sq. km.)	Percentage
Barren Land	1.88	0.005
Built Up Area	55.41	0.140
Vegetation	325.23	0.820
Water Bodies	14.20	0.035
Total	396.72	1.00

5.2 Land Surface Temperature

The situation of land use land cover of 10th March, 2020 was analyzed. Distribution of Land surface Temperature (LST) of that day was also determined. Analyzed the relationship between land use land cover and LST using derived values. The situation of land use land cover, and Land surface temperature obtained using remote sensing and GIS technique. Each image pixel represents the surface temperature of each object that may be group of numerous land cover types. By using above mentioned processing steps for LANDSAT 8 data LST maps are generated independently for the thermal band 10. Retrieved Land Surface Temperature of band 10 maps for the dates 10-03-2020 of Kathmandu, Bhaktapur and Lalitpur districts are shown in the figure 7, figure 8 and figure 9 respectively. NDVI maps of the study area for the day 10-03-2020 of Kathmandu, Bhaktapur and Lalitpur districts are shown in the figure 10, figure 11, and figure 12 respectively. Maximum, minimum, mean and standard deviation value of LST of Kathmandu, Bhaktapur, and Lalitpur district are shown in table 6, table 7, and table 8 respectively. Maximum, minimum, mean and standard deviation value of NDVI of Kathmandu, Bhaktapur, and Lalitpur districts are presented in tables 9, table 10, and table 11 respectively. Spatial spreading of surface temperature are maifested in LST maps. From these maps it is observed that different land cover types are having various temperature values due to variations in physical characteristics of the land covered by the different objects.

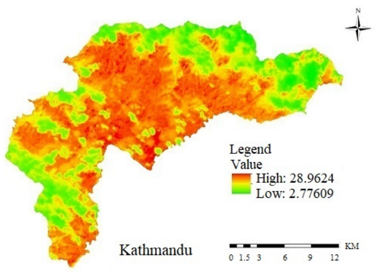

Figure 7: Land Surface Temperature map of Kathmandu district

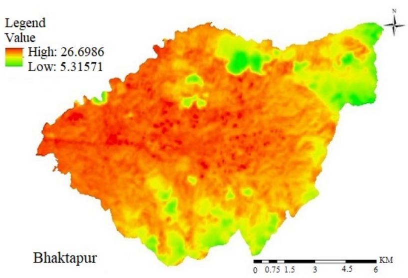

Figure 8: Land Surface Temperature map of Bhaktapur district

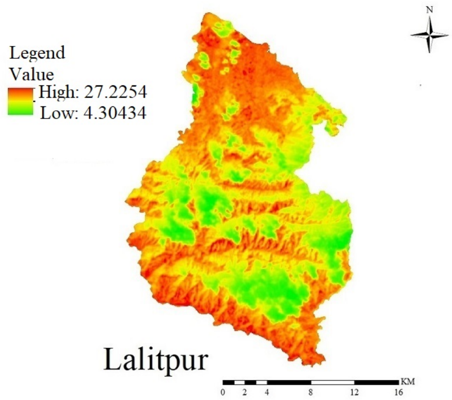

Figure 9: Land Surface Temperature map of Lalitpur district

Table 6: Land Surface Temperature parameters of Kathmandu district: 10th March, 2020

Parameters	Degree Celsius
Maximum	28.96244049
Minimum	2.776094675
Mean	15.92923993
Standard Deviation	5.944068717

Table 7: Land Surface Temperature parameters of Bhaktapur district: 10th March, 2020

Parameters	Degree Celsius
Maximum	26.69861412
Minimum	5.315711021
Mean	18.63532301
Standard Deviation	3.642881158

Table 8: Land Surface Temperature parameters of Lalitpur district: 10th March, 2020

Parameters	Degree Celsius
Maximum	27.22535706
Minimum	4.304338455
Mean	16.48618861
Standard Deviation	4.789573931

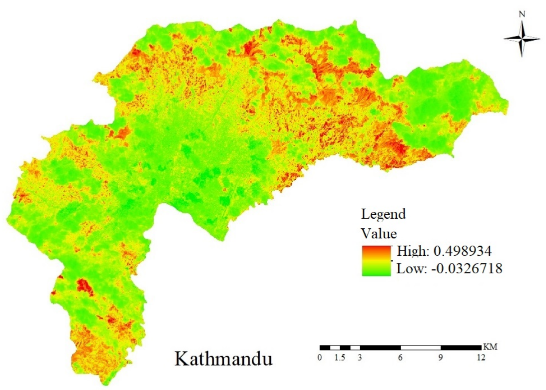

Figure 10: NDVI of Kathmandu district

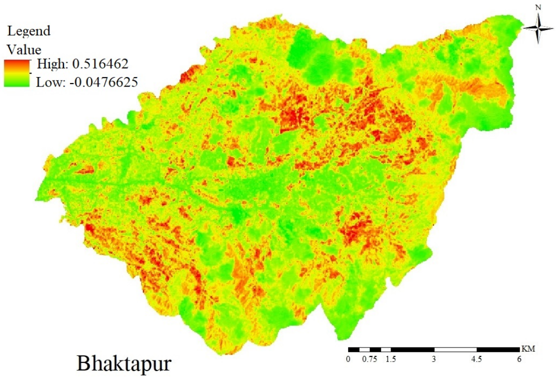

Figure 11: Normalized Difference Vegetation Index (NDVI) of Bhaktapur district

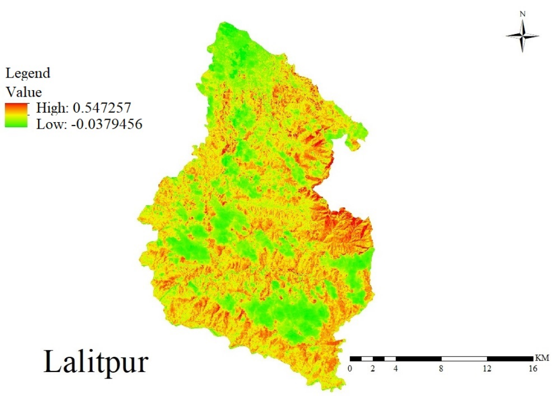

Figure 12: Normalized Difference Vegetation Index (NDVI) of Kathmandu district

Table 9: Normalized Difference Vegetation Index (NDVI) parameters of Kathmandu district: 10th March, 2020

Parameters	Value
Maximum	0.498933971
Minimum	-0.032671798
Mean	0.15381279
Standard Deviation	0.096198268

Table 10: Normalized Difference Vegetation Index (NDVI) parameters of Bhaktapur district: 10th March, 2020

Parameters	Value
Maximum	0.51646167
Minimum	-0.047662456
Mean	0.206864557
Standard Deviation	0.096541251

Table 11: Normalized Difference Vegetation Index (NDVI) parameters of Lalitpur district: 10th March, 2020

Parameters	Value
Maximum	0.547257245
Minimum	-0.037945628
Mean	0.210005047
Standard Deviation	0.09922092

5.3 Validation

The objective of this work is that, estimation and validation of LST from the LANDSAT 8 image with in-suite data obtained from 6 Weather Station of Kathmandu district. Mono Window algorithm is the must suggested technique to estimation. Also, Split window algorithm method can be used to estimate LST by using band 10 thermal image [40].Weather station temperature are used to validate land surface temperature of study areas [41]. This study considers band 10 thermal image for LST calculation. The obtained LST result is compared with weather station temperature statistical analysis is done by calculating correlation coefficient between retrieved LST from band 10 and in-suite weather station data [42]. And also with reference to comparison is performed through LST of band 10 and the proposed method. Table 12 represent the Land Surface Temperature (LST) retrieved by using Band 10 by using Mono Window Algorithm and station data for 10-03-2020.

Table 12: Remote sensing temperature vs weather station temperature on 10th March, 2020

Location	LSTmax	LSTmin	Tmax	Tmin
Airport	28.96	7.20	24.5	11.9
Panipokhari	24.69	14.54	24.5	13.2
Khumaltar	23.36	10.15	23.6	11.4
Godavari	23.40	6.88	20	5.8
Changunaryan	26.13	5.72	24.4	8.4
Nagarkot	20.44	6.23	18	7.3

The correlation coefficient of weather station temperature data with LST retrieved by using band 10 for maximum and minimum temperatures are 0.80 and 0.74 respectively.. The correlation coefficient can be estimated by using equation (8).

r= correl(x,y)

$$r = \frac{\sum_{i=1}^{n}(x_i - \bar{x})(y_i - \bar{y})}{\sum_{i=1}^{n}(x_i - \bar{x})^2(y_i - \bar{y})^2} \tag{8}$$

Figure 13 shows plotting of retrieved LST and weather station temperature data for the study area by using band 10 for the day 10th March 2020. From the plot it can be witnessed that the retrieved LST using band10 is having slight deviation compared to weather data from the study area for the chosen 6 weather stations.

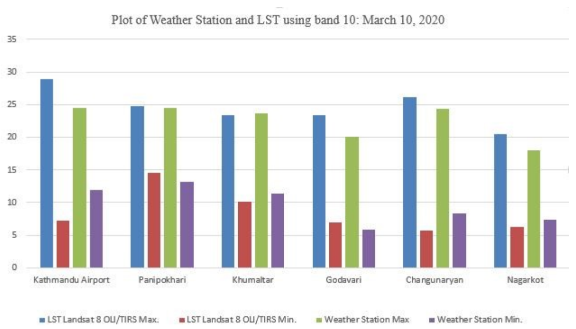

Figure 13: Plot of weather station and remote sensing temperature of Kathmandu valley

5.4 Urban Heat Island

Figure 14, figure 15, and figure 16 shows urban heat island distribution in Kathmandu, Bhaktapur, and Lalitpur districts respectively. UHI graph profile of Kathmandu, Bhaktapur, and Lalitpur of 10th March, 2020 is shown in the figure 17, figure 18, and figure 19 respectively. Urban Heat Island graph profile from south-west to east-north of Kathmandu valley is shown in the figure 17. UHI value of Kathmandu district ranges from -2.21286 °C to 2.19264 °C, positive and higher values corresponds to the nearby densely built up areas and central zone of the Kathmandu district, whereas vegetative and forest areas are experiencing negative UHI. Bhaktapur district has dense urbanization in western and central zone. UHI graph profile of Bhaktapur district is shown in figure 18. UHI value of Bhaktapur district ranges from -3.65634 °C to 2.21344 °C, where, most positive value correspond western and central zone, whereas negative value corresponds east-north and southern zones. Lalitpur district has large dense forests in the southernmost part with scattered dense built up areas in southern areas, whereas northern part has large dense built up areas. Figure 19 shows the UHI graph profile of Lalitpur district, where UHI values ranges from -2.54341 °C to 2.2422 °C. Due to large dense forest and scattered built up areas in the southern areas UHI value highly fluctuates in the southern zone, where positive values are found in built up areas, whereas negative value lies in forest and vegetative areas. As southern area has large built up areas, UHI value continues to positive values. Thus to Higher values of UHI corresponds to the built up and urbanized areas of kathmandu valley, whereas lower values corresponds to vegetative and forest areas. Higher proportion of distribution of UHI lies in the inner urban areas, where as distribution of UHI is low in outer rural areas. It is because of surrounding rural areas has more vegetation as compared to central urban areas of Kathmandu valley.

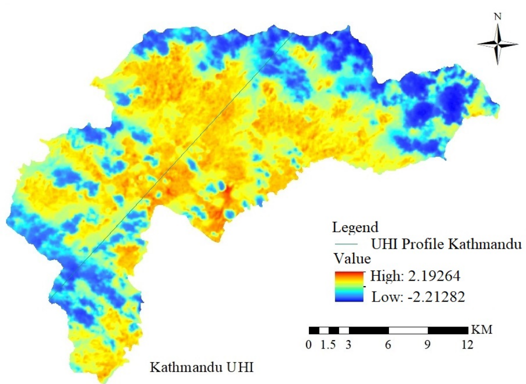

Figure 14: Urban Heat Island (UHI) map of Kathmandu district

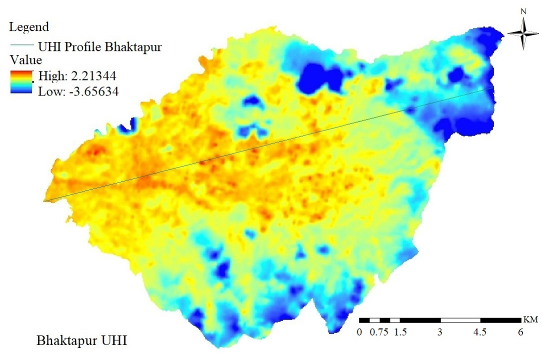

Figure 15: Urban Heat Island (UHI) map of Bhaktapur district

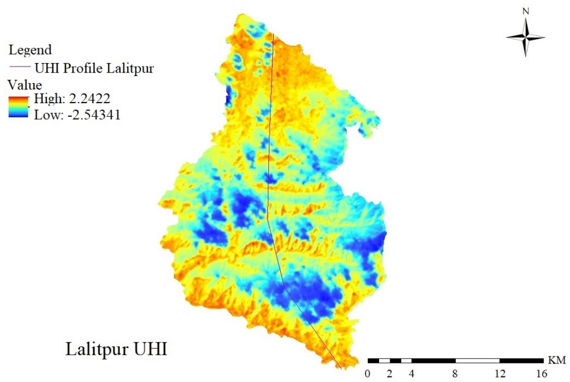

Figure 16: Urban Heat Island (UHI) map of Lalitpur district

Table 13: Urban Heat Island (UHI) parameters of Kathmandu district: 10th March, 2020

Parameters	Value
Maximum	2.192639589
Minimum	-2.212818623
Mean	-4.98E-08
Standard Deviation	0.999999968

Table 14: Urban Heat Island (UHI) parameters of Bhaktapur district: 10th March, 2020

Parameters	Value
Maximum	2.213438034
Minimum	-3.656339884
Mean	1.20E-07
Standard Deviation	1.000000001

Table 15: Urban Heat Island (UHI) parameters of Lalitpur district: 10th March, 2020

Parameters	Value
Maximum	2.242196798
Minimum	-2.543409824
Mean	-5.79E-08
Standard Deviation	0.999999955

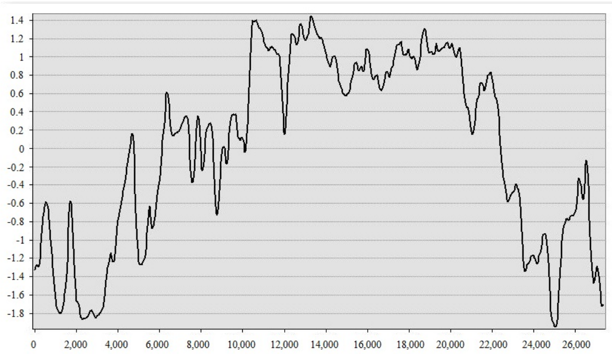

Figure 17: Urban Heat Island (UHI) profile graph of Kathmandu district

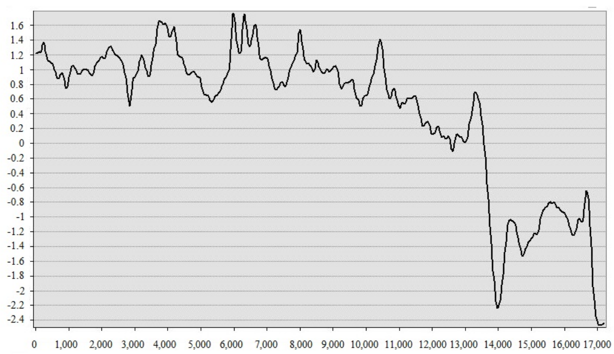

Figure 18: Urban Heat Island (UHI) profile graph of Bhaktapur district

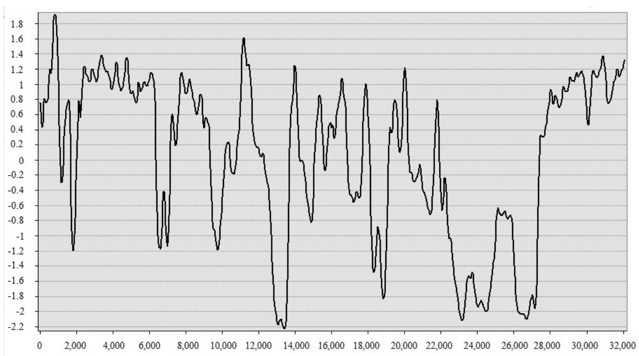

Figure 19: Urban Heat Island (UHI) profile graph of Lalitpur district

6. Conclusion

Kathmandu, Bhaktapur and Lalitpur districts LST variation were analyzed using data of Landsat 8 satellite. Land cover classficication and NDVI values were also calculated to analyze the distribution of LST values in Kathmandu, Bhaktapur and Lalitpur districts. LST value corresponding to lower NDVI value and dense built up areas is high, whereas low in areas with higher NDVI value and scattered and dense vegetation. Calculated UHI values were found to be proportional to anthropogenic activity areas. This happen because physical properties of the urban areas influence albedo composition of the city, that rises the temperature.

This research work considered 6 weather stations as validation points from study area for the validation purpose. The LST was calculated using Mono Window Algorithm. Here, thermal band 10 of TIR sensor of LANDSAT 8 is used. The estimated LST using remote sensing and ArcGIS were validated by in-suite measures taken from same geographical locations. And also both observations consider same date. Here for the proposed work estimation satellite data considered date 10-03-2020. Little deviation has been observed when compared to estimated LST using band 10 with weather station data. This is due to cloud covers and spatial resolution of the satellite images.

Acknowledgments

Authors are thankful to the technical assistance and support from the Department of Applied Science and Chemical Engineering, Pulchowk Campus. The authors are also thankful to the USGS Earth Explorer for providing Landsat 8 images to carry out this research work. Also the Authors wishes thank to the Department of Hydrology and Meteorology for providing weather station temperature data which are used for validation of this research work.

References

[1] Mingliang Liu and Hanqin Tian. China's land cover and land use change from 1700 to 2005: Estimations from high-resolution satellite data and historical archives. *Global Biogeochemical Cycles*, 24(3), 2010.

[2] Noyingbeni Kikon, Prafull Singh, Sudhir Kumar Singh, and Anjana Vyas. Assessment of urban heat islands (uhi) of noida city, india using multi-temporal satellite data. *Sustainable Cities and Society*, 22:19–28, 2016.

[3] James A Voogt and Tim R Oke. Thermal remote sensing of urban climates. *Remote sensing of environment*, 86(3):370–384, 2003.

[4] Timothy R Oke. The energetic basis of the urban heat island. *Quarterly Journal of the Royal Meteorological Society*, 108(455):1–24, 1982.

[5] Parham A Mirzaei and Fariborz Haghighat. Approaches to study urban heat island–abilities and limitations. *Building and environment*, 45(10):2192–2201, 2010.

[6] Arthur H Rosenfeld, Hashem Akbari, Sarah Bretz, Beth L Fishman, Dan M Kurn, David Sailor, and Haider Taha. Mitigation of urban heat islands: materials, utility programs, updates. *Energy and buildings*, 22(3):255–265, 1995.

[7] Claire Sarrat, Aude Lemonsu, Valéry Masson, and D Guedalia. Impact of urban heat island on regional atmospheric pollution. *Atmospheric environment*, 40(10):1743–1758, 2006.

[8] Haider Taha. Urban climates and heat islands: albedo, evapotranspiration, and anthropogenic heat. *Energy and buildings*, 25(2):99–103, 1997.

[9] Kimberly A Gray and Mary E Finster. The urban heat island, photochemical smog, and chicago: Local features of the problem and solution. *Department of Civil Engineering, Northwestern University, Evanston, IL*, 2000.

[10] P Krishna Rao. Remote sensing of urban" heat islands" from an environmental satellite. *Bulletin of the American meteorological society*, 53(7):647–648, 1972.

[11] Cathy Aniello, Ken Morgan, Arthur Busbey, and Leo Newland. Mapping micro-urban heat islands using landsat tm and a gis. *Computers & Geosciences*, 21(8):965–969, 1995.

[12] CP Lo and Dale A Quattrochi. Land-use and land-cover change, urban heat island phenomenon, and health implications. *Photogrammetric Engineering & Remote Sensing*, 69(9):1053–1063, 2003.

[13] Hao Zhang, Zhi-fang Qi, Xin-yue Ye, Yuan-bin Cai, Wei-chun Ma, and Ming-nan Chen. Analysis of land use/land cover change, population shift, and their effects on spatiotemporal patterns of urban heat islands in metropolitan shanghai, china. *Applied Geography*, 44:121–133, 2013.

[14] Benedicte Dousset and Françoise Gourmelon. Satellite multi-sensor data analysis of urban surface temperatures and landcover. *ISPRS journal of photogrammetry and remote sensing*, 58(1-2):43–54, 2003.

[15] Susan Solomon. Ipcc (2007): Climate change the physical science basis. In *Agu fall meeting abstracts*, volume 2007, pages U43D–01, 2007.

[16] Aneesh Mathew, Sumit Khandelwal, and Nivedita Kaul. Investigating spatial and seasonal variations of urban heat island effect over jaipur city and its relationship with vegetation, urbanization and elevation parameters. *Sustainable cities and society*, 35:157–177, 2017.

[17] M Tiangco, AMF Lagmay, and J Argete. Aster-based study of the night-time urban heat island effect

in metro manila. *International Journal of Remote Sensing*, 29(10):2799–2818, 2008.

[18] Nicholas Clinton and Peng Gong. Modis detected surface urban heat islands and sinks: Global locations and controls. *Remote Sensing of Environment*, 134:294–304, 2013.

[19] Yupeng Wang and Hashem Akbari. Analysis of urban heat island phenomenon and mitigation solutions evaluation for montreal. *Sustainable Cities and Society*, 26:438–446, 2016.

[20] Lisette Klok, Sander Zwart, Henk Verhagen, and Elena Mauri. The surface heat island of rotterdam and its relationship with urban surface characteristics. *Resources, conservation and recycling*, 64:23–29, 2012.

[21] Sumit Khandelwal and Rohit Goyal. Effect of vegetation and urbanization over land surface temperature: case study of jaipur city. In *EARSeL Symposium*, pages 177–83, 2010.

[22] John Bongaarts. United nations department of economic and social affairs, population division world mortality report 2005. *Population and Development Review*, 32(3):594–596, 2006.

[23] Hao Zhang, Zhi-fang Qi, Xin-yue Ye, Yuan-bin Cai, Wei-chun Ma, and Ming-nan Chen. Analysis of land use/land cover change, population shift, and their effects on spatiotemporal patterns of urban heat islands in metropolitan shanghai, china. *Applied Geography*, 44:121–133, 2013.

[24] F Sattari and M Hashim. A brief review of land surface temperature retrieval methods from thermal satellite sensors. *Middle-East Journal of Scientific Research*, 22(5):757–768, 2014.

[25] Fei Wang, Zhihao Qin, Caiying Song, Lili Tu, Arnon Karnieli, and Shuhe Zhao. An improved mono-window algorithm for land surface temperature retrieval from landsat 8 thermal infrared sensor data. *Remote sensing*, 7(4):4268–4289, 2015.

[26] A Rajani and S Varadarajan. Lu/lc change detection using ndvi & mlc through remote sensing and gis for kadapa region. In *Cognitive Informatics and Soft Computing*, pages 215–223. Springer, 2020.

[27] S Narayana Reddy and B Manikiam. Land surface temperature retrieval from landsat data using emissivity estimation. *International Journal of Applied Engineering Research*, 12(20):9679–9687, 2017.

[28] Parmeshwar Udmale, Hiroshi Ishidaira, Bhesh Raj Thapa, and Narendra Man Shakya. The status of domestic water demand: supply deficit in the kathmandu valley, nepal. *Water*, 8(5):196, 2016.

[29] Reilly Brooks. Relocation, resistance and resilience: squatter community responses to government intervention for urban development in kathmandu. *University of Tsukuba. Graduate School of Life and Environmental Sciences, University of Tsukuba, Japan*, page 153, 2016.

[30] Rajesh Bahadur Thapa. Spatial process of urbanization in kathmandu valley, nepal. *Independent Study Project*, 2016.

[31] Elisa Muzzini and Gabriela Aparicio. *Urban growth and spatial transition in Nepal: An initial assessment*. World Bank Publications, 2013.

[32] MoUD. *National Urban Development Strategy 2015. Kathmandu: Ministry of Urban Development, Government of Nepa*. http://www.moud.gov.np/pdf/NUDS-2015-final-draft.pdf, 2015.

[33] Pushkar K Pradhan. Population growth, migration and urbanisation. environmental consequences in kathmandu valley, nepal. In *Environmental change and its implications for population migration*, pages 177–199. Springer, 2004.

[34] Inu Pradhan-Salike and Jiba Raj Pokharel. Impact of urbanization and climate change on urban flooding: a case of the kathmandu valley. *JNRD-Journal of Natural Resources and Development*, 7:56–66, 2017.

[35] Rajesh Bahadur Thapa, Yuji Murayama, and Shailja Ale. Kathmandu. *Cities*, 25(1):45–57, 2008.

[36] USGS. *Landsat 8*. https://www.usgs.gov, 2021.

[37] Mengmeng Wang, Guojin He, Zhaoming Zhang, Guizhou Wang, Zhihua Wang, Ranyu Yin, Shiai Cui, Zhijie Wu, and Xiaojie Cao. A radiance-based split-window algorithm for land surface temperature retrieval: Theory and application to modis data. *International Journal of Applied Earth Observation and Geoinformation*, 76:204–217, 2019.

[38] Ugur Avdan and Gordana Jovanovska. Algorithm for automated mapping of land surface temperature using landsat 8 satellite data. *Journal of sensors*, 2016, 2016.

[39] Thomas Lillesand, Ralph W Kiefer, and Jonathan Chipman. *Remote sensing and image interpretation*. John Wiley & Sons, 2015.

[40] Juan-Carlos Jiménez-Muñoz and José A Sobrino. Split-window coefficients for land surface temperature retrieval from low-resolution thermal infrared sensors. *IEEE geoscience and remote sensing letters*, 5(4):806–809, 2008.

[41] Darren How Jin Aik, Mohd Hasmadi Ismail, and Farrah Melissa Muharam. Land use/land cover changes and the relationship with land surface temperature using landsat and modis imageries in cameron highlands, malaysia. *Land*, 9(10):372, 2020.

[42] A Rajani and S Varadarajan. Estimation and validation of land surface temperature by using remote sensing & gis for chittoor district, andhra pradesh. *Turkish Journal of Computer and Mathematics Education (TURCOMAT)*, 12(5):607–617, 2021.